Ultra-compact silicon nanophotonic modulator based on electro-optic polymer infiltrated slot photonic crystal waveguide

Che-Yun Lin[1], Beomsuk Lee[1], Alan X. Wang[2], Wei-Cheng Lai[1]
, Swapnajit Chakravarty[2], Yazhao Liu[1], David Kwong[1]
, Ray T. Chen[1*], Jingdong Luo[3], and Alex K.Y Jen[3]
[*]Email: raychen@uts.cc.utexas.edu

[1]The University of Texas at Austin, 10100 Burnet Rd. Bldg 160MER, Austin, TX-78758, USA
[2]Omega Optics, Inc. 10435 Burnet Road, Suite 108, Austin, TX 78758
[3]The University of Washington at Seattle, Materials Science and Engineering Dept. Box 352120, Seattle, WA 98195-2120

ABSTRACT

We experimentally demonstrate a Mach-Zehnder modulator based on electro-optic (EO) polymer (AJ-CKL1/PMMA) infiltrated photonic crystal slot waveguide. The modulator design combines the advantage of excellent optical confinement in silicon slot waveguide, slow light enhancement in photonic crystal waveguide, and strong electro-optical response in EO polymer. This design allows us to achieve electro-optic modulation in active region only 352μm long. Matching the mode profile and group velocity between strip and photonic crystal slot waveguide enables coupling into slow light regime. The modulator shows a 22V switching voltage and an improved in-device EO coefficient of 51pm/V as compared to recently reported value.

Keywords: silicon photonics, photonic crystals, slot waveguide, electro-optic polymer, and electro-optic modulator

1. INTRODUCTION

Optical modulation in silicon usually involves active tuning of refractive index based on perturbation of carrier concentration [1] or thermal optic effect [2]. These modulation mechanisms work well in low speed optical systems as they offer compact size and low power consumption as compared to conventional photonic devices. With the development of electro-optic polymer, it is shown that the electro-optic coefficient could well exceed 300pm/V [3] and the electro-optic response can be extended up to THz range [4]. Electro-optic modulator based on silicon-EO polymer hybrid system is therefore a promising approach as it combines the strong optical confinement of silicon, mature processing technology, and the strong and fast EO response of EO polymer.

Photonic crystals are periodic dielectric structures that can guide and manipulate light at the scale of optical wavelength [5-8]. These artificial crystals derive their properties not from their atomic composition, but from their geometrical structure. This novel property allows device engineers to design the way light interacts with these artificial crystals by changing their geometry. One example of this novel property is to create slow light in photonic crystals. It has been reported that light can be slowed down by a factor of 100 as compared to the speed of light in vacuum when it is guided near the band edge of the defect mode [5]. When light slows down, the optical energy is spatially compressed, which results in strong enhancement of field intensity. Many nonlinear phenomena will be enhanced under the presence of slow light, which allows us to design very compact electro-optic modulator based on this field enhancement. Slot waveguides in silicon [9] has the unique property of guiding and confining light in the low index region with strong field enhancement. Due to the high refractive index discontinuity at the silicon-low index material interface, TE-component of electric field is enhanced by a factor of $(n_{si}/n_{low})^2$. Merging the benefit of slow light in photonic crystal waveguide, strong optical confinement in slot waveguide, and the strong electro-optic effect in EO polymer, we experimentally demonstrate a Mach-Zehnder modulator based on EO polymer (AJ-CKL1/PMMA) infiltrated silicon photonic crystal slot waveguide with a compact interaction length of 352μm.

Optoelectronic Interconnects and Component Integration IX, edited by Alexei L. Glebov, Ray T. Chen,
Proc. of SPIE Vol. 7607, 76070D · © 2010 SPIE · CCC code: 0277-786X/10/$18 · doi: 10.1117/12.843884

2. DESIGN OF PHOTONIC CRYSTAL SLOT WAVEGUIDE

1.1 Design photonic crystal slot waveguide

The design parameters and photonic band diagram of our design is shown in Figure 1 (a) and (b). From the band diagram, we can see that the defect mode spans the normalized frequency range from a/λ=0.246 to 0.251. This corresponds to a wavelength range from 1534nm to 1566nm. Transmission around 1566nm should reveal a sharp decrease as wavelength decreases due to the presence of photonic bandgap [5]. By contrast, the transmission around 1534nm would show a smoother cutoff due to the failure of light line confinement. As the band diagram shows, for wavelength close to the band edge around 1566nm, the slope of the defect mode becomes nearly flat, and the group index increases rapidly to over 100 as presented in Figure 1 (c). This high group index indicates the field concentration of the guided mode is greatly enhanced around λ=1566nm (Figure 1 (d)), which will significantly enhance the electro-optic efficiency of our device [10-12].

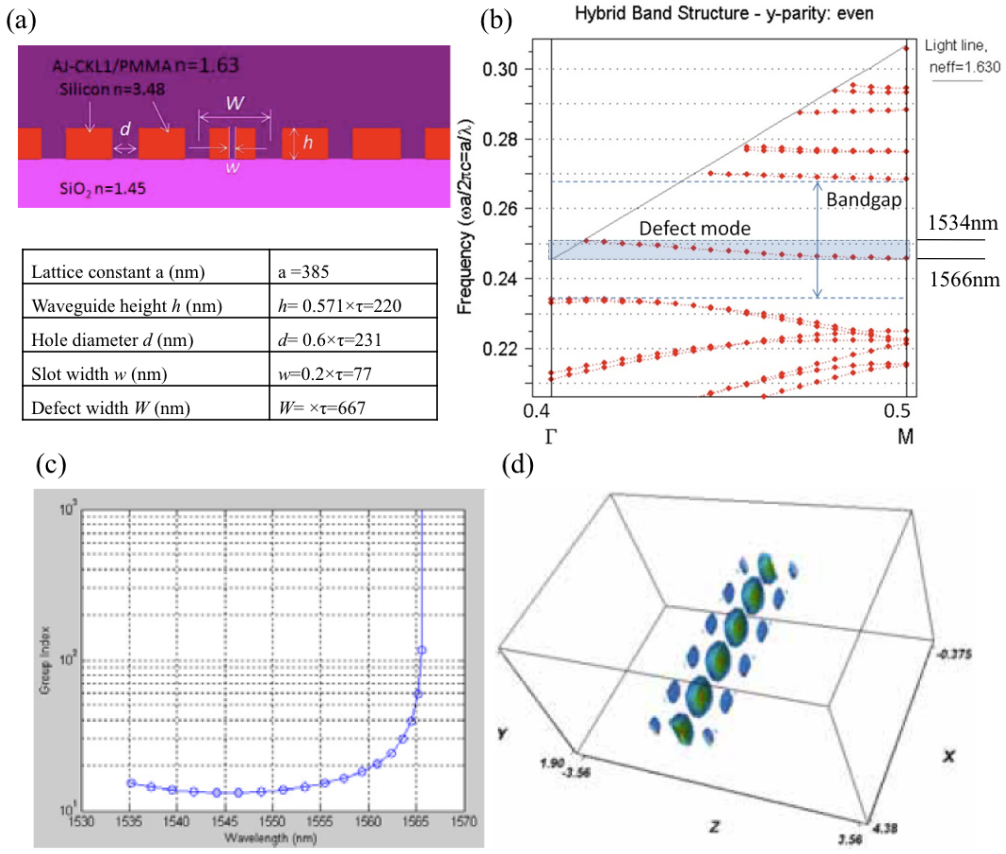

Lattice constant a (nm)	a =385
Waveguide height *h* (nm)	*h*= 0.571×τ=220
Hole diameter *d* (nm)	*d*= 0.6×τ=231
Slot width *w* (nm)	*w*=0.2×τ=77
Defect width *W* (nm)	*W*= ×τ=667

Figure 1. (a) Summary of the design parameters and the schematic illustration each parameters. (b) Photonic band diagram of the photonic crystal slot waveguide. (c) Group index (n_g) as a function wavelength. (d) Field distribution around 1566nm wavelength, which shows majority of the field is concentrated in the EO polymer-filled slot.

1.2 Design of mode converter and photonic crystal taper

Light coupling into photonic crystal slot waveguide in slow light regime could be challenging due to the following reasons: First, the exotic mode profile of photonic crystal slot waveguide shows huge mode mismatch with the input strip waveguide, which results in negligible coupling without careful design. Second, the group velocity mismatch between strip waveguide and slow light photonic crystal slot waveguide causes huge reflection at the interface. Several approaches have been proposed to address coupling from strip to slot waveguide [13, 14] and from strip to photonic crystal waveguide [15-17]. However, coupling into slow light photonic crystal slot waveguide still need to be developed. Combining the advantages of the above coupling approaches, we developed a micro mode converter that is capable of

converting the strip waveguide mode to a profile resembling photonic crystal slot waveguide mode. In addition, a photonic crystal taper is added to solve the group velocity mismatch problem. The schematic of mode converter, photonic crystal taper (or impedance taper), and active slow light region is shown in Figure 2 (a). When input light enters the mode converter from strip waveguide, it is gradually squeezed into narrower profile and partially coupled to the side tips at the same time. As the light travels through the mode converter, the intensity profile is converted to a profile that resembles slot photonic crystal waveguide mode, which reduces the mode mismatch significantly. In the photonic crystal taper region, the defect width is gradually narrowed from W1.08 to W1.02 before the active region. Here W1.08 refers the width of the defect is equal to lattice constant times $\sqrt{3}$ times 1.08. As Figure 2 (b) shows, the group index (n_g) of the crystal lattice increases gradually from 14 (W1.08) to 30 (W1) for the wavelength around 1560nm near the band edge. This gradual increase in group index allows light to slow down period by period as it enters deeper into the photonic crystal hence reduces the mismatch in the group velocity. Coupling the light out into the strip waveguide is simply the reversed process. We also simulate the transmission spectrum of such photonic crystal slot waveguide with and without photonic crystal impedance taper. As the red curve in Figure 2 (d) shows, for the waveguide without impedance taper, the transmission shows Fabry-Perot resonances due to the reflection at the interface. Moreover, the transmission for waveguide without taper drops gradually while approaching the band edge, which results in a negligible coupling around band edge. By contrast, the transmission for the waveguide that has impedance taper remains high when approaching the band edge, and finally drops sharply due to the presence of photonic bandgap. By means of combining the mode converter and impedance taper, the total coupling efficiency is almost 50% (<3dB loss).

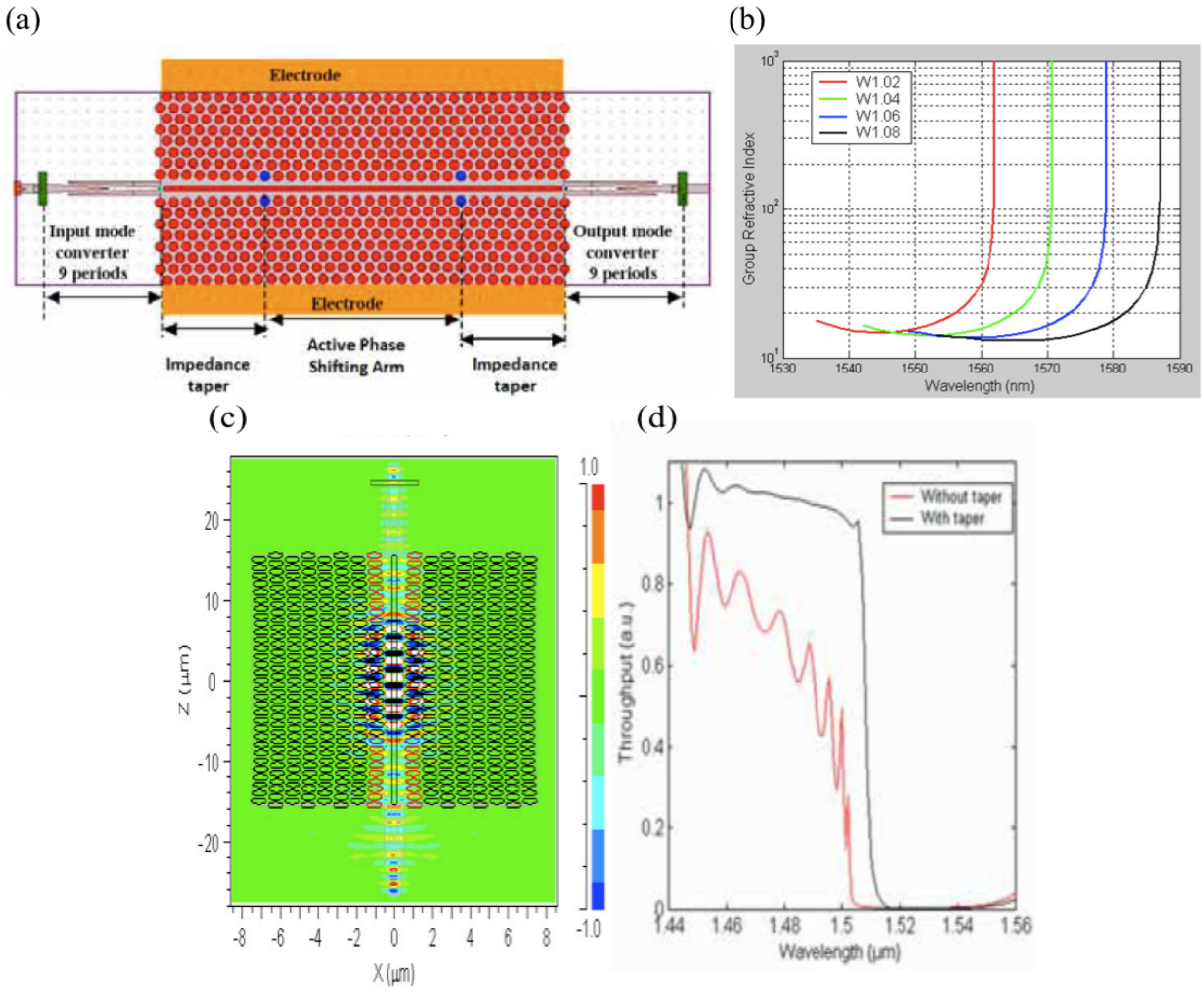

Figure 2. (a) Schematic of the micro mode converter, impedance taper, and active slow light region. The input and output end of the device are symmetrical. (b) Design of photonic crystal taper. (c) 2D finite-difference time domain (FDTD) simulation under continuous wave (CW) excitation. Mode conversion in the mode converter region and the gradual "slow down" are shown. (d) Comparison of transmission with and without photonic crystal taper.

3. DEVICE FABRICATION

Modulator devices were fabricated on Unibond SOI wafer manufactured by SOITECH with 250nm thick silicon layer and a 3μm thick buried oxide (BOX) layer. The thick BOX layer serves as bottom cladding of slot photonic crystal waveguide, which prevents optical mode leakage through the substrate. 20nm of the silicon layer was oxidized for an hour and fifty minutes to grow 45nm thick thermal oxide as a hard mask for pattern transfer. The slot photonic crystal waveguide, photonic crystal impedance tapers, mode converters, and input/output strip waveguides were patterned in one step, using JEOL JBX-6000FS 50kV electron beam lithography system. After developing the sample, the resist pattern was transferred to the oxide hard mask using reactive ion etching (RIE) using CHF_3/O_2 chemistry. The oxide hard mask pattern was then transferred to 230nm-thick silicon device layer using HBr/Cl_2 chemistry. The silicon etch rate was measured to be 55nm/min. This process guarantees nearly 90-degree sidewall profile with low sidewall roughness, which is estimated to be in the order of 10nm under SEM inspection as shown in Figure 3 (a) and (b). After silicon etching, the electrode was patterned by photolithography followed by metal deposition and lift off. The fabricated electrode structure is shown in Figure 3 (c). Finally, the photonic crystal slot waveguide structure was infiltrated with a guest/host electro-optic (EO) polymer (AJ-CKL1 25% wt. in PMMA using 1,1,2-trichloroethane as solvent). The EO polymer solution was spun onto the photonic crystal structure followed by overnight baking at 80°C in order to remove residual solvent and bubbles in the film. The cross-sectional SEM shows that the slot can be seamlessly filled with slot as narrow as 100nm.

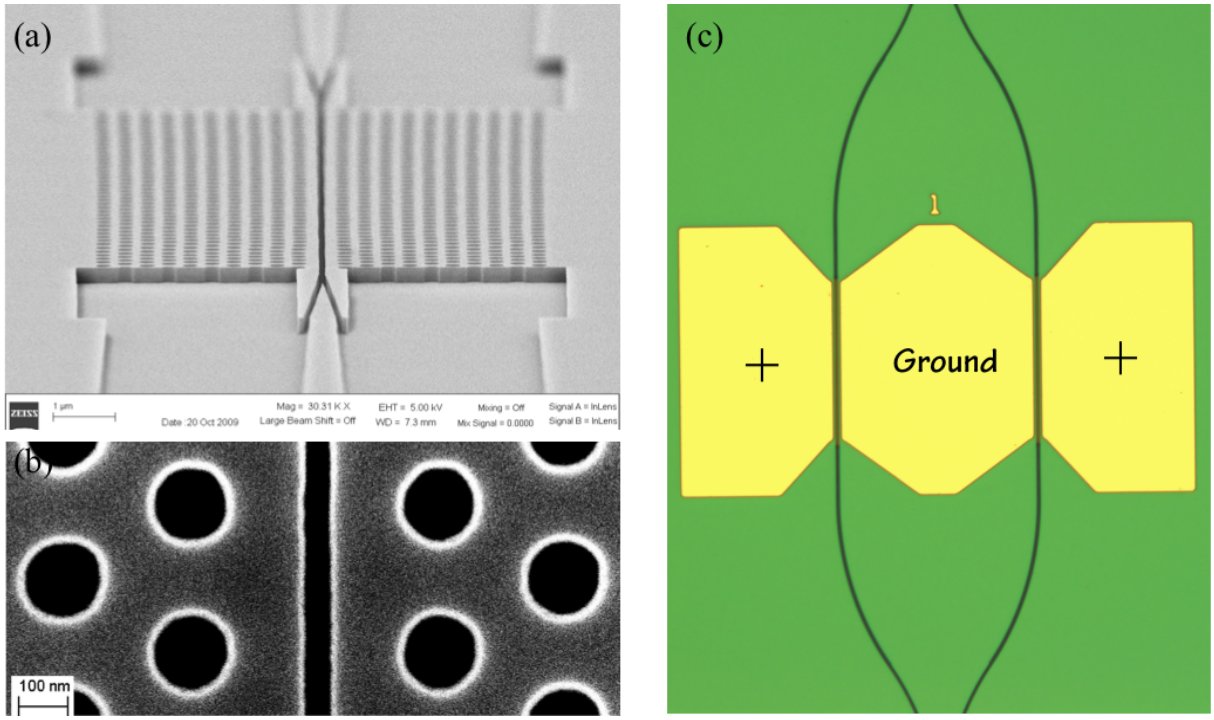

Figure 3. (a) Scanning electron microscope (SEM) picture of the tilted view of fabricated silicon slot photonic crystal waveguide. (b) Zoom-up view of the slot and first two rows of holes. (c) Electrode structure after metal deposition and lift off.

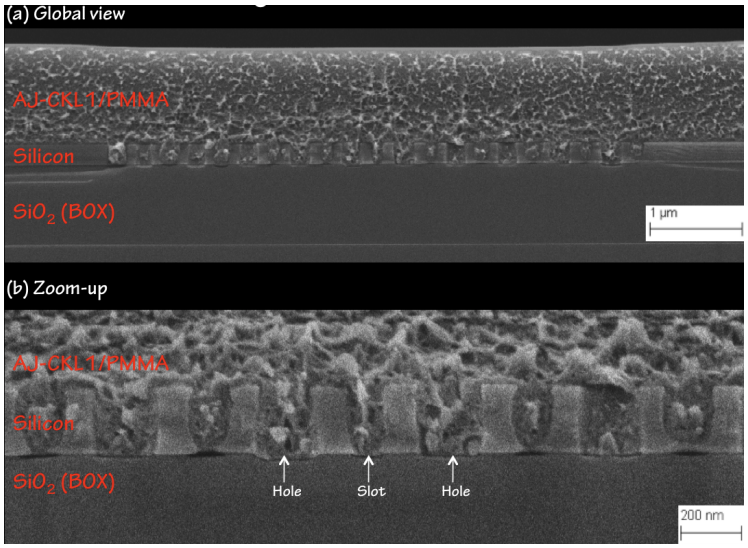

Figure 4. SEM picture of the silicon photonic crystal slot waveguide after infiltration of guest host EO polymer (AJ-CKL1/PMMA). It is clearly seen that the holes and slot can be seemly filled by EO polymer. Before taking SEM picture, the sample was dipped in buffered HF solution for a few seconds to etch away 10nm of the buried oxide to better display the interface between silicon and SiO2 (a) Overall view of the entire cross-section of photonic crystal slot waveguide. (b) Zoom-up view of the slot region.

4. POLING OF EO POLYMER

The key for enabling electro-optic modulation in silicon is to create electro-optic effect in the EO polymer infiltrated slot. This is achieved by aligning of the NLO-chromophores with external electric field. The silicon photonic crystal can also function as electrode during poling process. This is confirmed by resistance measurement between the gold electrodes on a dummy sample, which has the same device structure lacking a slot in the center of photonic crystal waveguide. The measured inter-electrode resistances are in the range of 4~8kΩ, which indicates that the voltage drop on silicon is negligible as compared to the voltage drop across the EO polymer-infiltrated slot. The poling setup is schematically explained in Figure 5 (a). During the poling process, the sample was heated to the glass transition temperature (T_g=90°C) of the guest/host polymer while 150V/μm of poling field was applied. At the glass transition temperature the chromophore molecules are free to move; therefore, it can be noncentrosymmetrically aligned with poling field. Upon reaching the glass transition temperature, the sample was then cooled down to room temperature, and the poling voltage was switched off thereby freeze the aligned molecules of the NLO-chromophore. Through this poling process, electro-optic effect in the slot region is created. Leakage current during poling is monitored in situ as shown in Figure 5 (b).

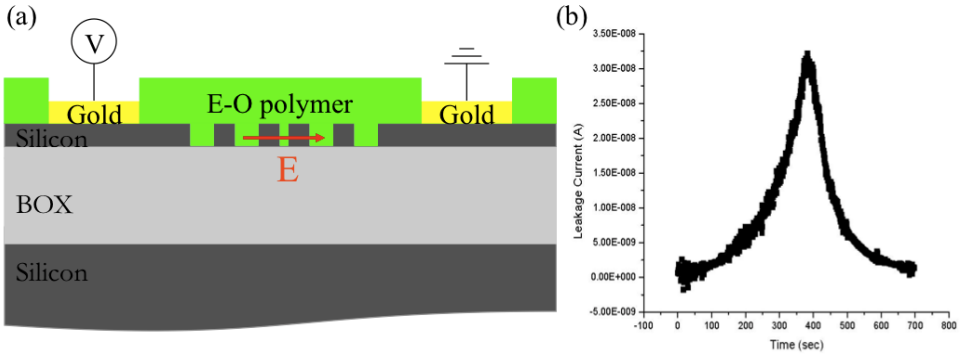

Figure 5. (a) Schematic of the poling setup. Poling voltage is applied to the gold electrode. The silicon photonic crystal also serves as electrode in the poling process. Because the resistance of silicon is very low compare to EO polymer, the poling electric field is

mainly concentrated on the slot region. (b) Leakage current during poling process. The sample was heated up from 30°C from t=0 at a ramp rate of 10°C/min. The leakage current peaked at glass transition temperature T_g=90°C around t=380sec, and then dropped rapidly with decreasing temperature.

5. OPTICAL TESTING

The fabricated MZ Modulator was tested on a Newport six-axis auto-aligning stage to facilitate light coupling. TE-polarized light from an external-cavity laser source was butt-coupled into the MZ modulator using tapered polarization maintaining fiber. The input laser light was polarized to achieve a TE/TM extinction ration of 20dB. The testing setup is shown schematically in Figure 6 (a). Figure 6 (b) shows the infrared image of MZ modulator when light is coupled. It is clearly seen that input light is launched into the MZ modulator, split into two individual arms, and coupled into the photonic crystal slot waveguide. The transmission spectrum in Figure 7 (b) was obtained using tunable laser. The modulation performance was characterized around 1495nm, which is consistent with the band edge of the observed defect mode. The long wavelength cut-off around 1499nm, which is due to the light line, is relatively smooth as compared to the short wavelength cutoff around 1493nm, which is the result of photonic bandgap cutoff. For wavelength longer than 1497nm, no high transmission peak was observed because of photonic bandgap. Another transmission peak was also found near 1488nm, which is mainly due to the light coupling from the slab mode. Based on the transmission spectrum, the electro-optic modulation was characterized at 1495nm near the band edge of the defect mode. We note that the measured defect mode is slightly shifted around 4nm away from the calculated result. We attribute this small discrepancy to the fabrication-induced disorder.

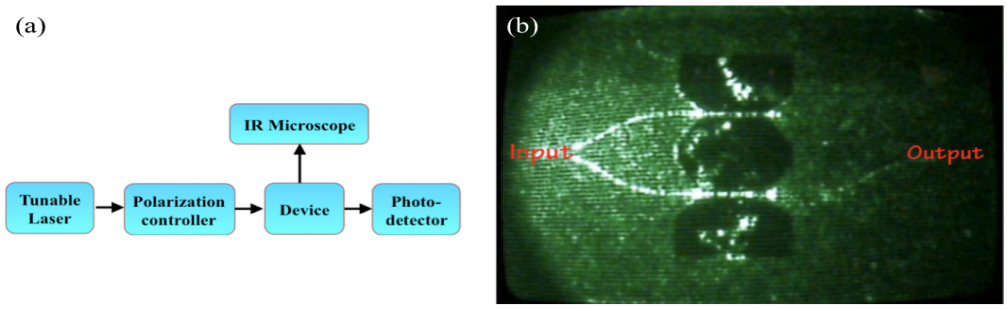

Figure 6. (a) Schematic of the light coupling setup. (b) IR microscope image from top view showing the light propagation along two arms of Mach-Zehnder modulator. Equal splitting of the light and light propagation inside the photonic crystal slot waveguide is clearly visible in the picture.

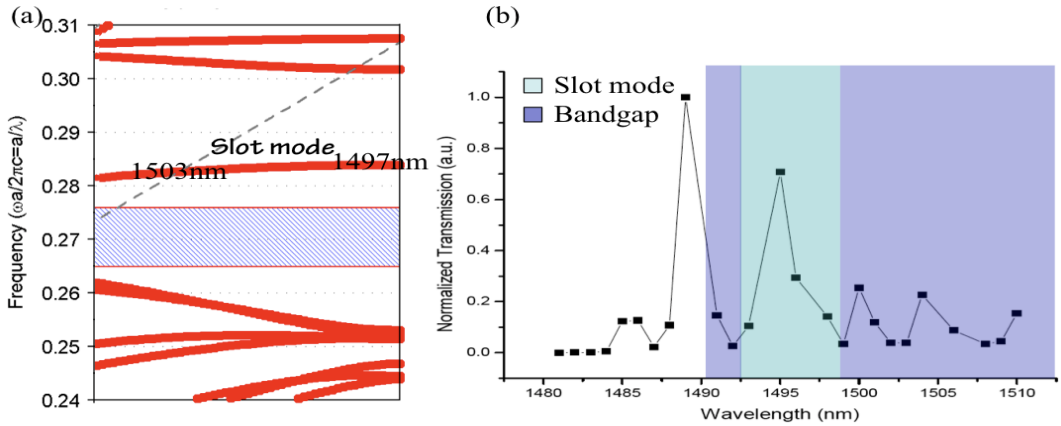

Figure 7. (a) Photonic band diagram calculated by BandSOFT based on plane wave expansion. (b) Transmission spectrum of the Mach-Zehnder modulator device.

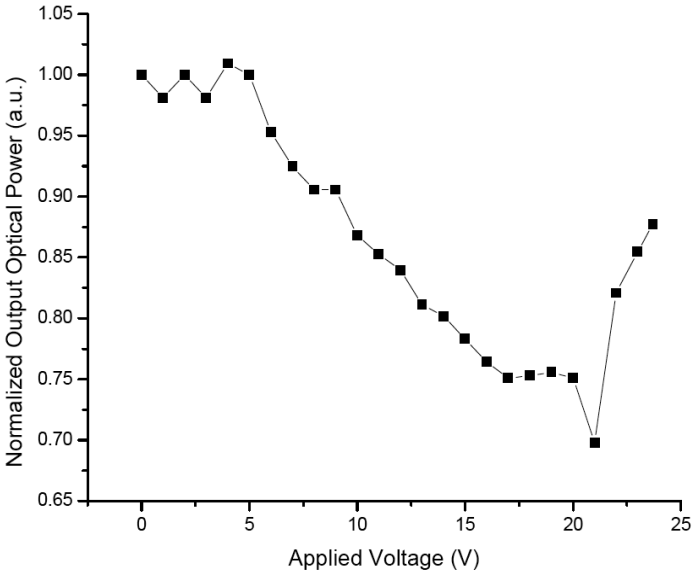

Figure 8. Output light intensity normalized to the maximum intensity as a function of applied voltage. The device shows a switching voltage around 22V

Modulation of output light is performed by applying modulation voltage across one arm of the MZ modulator. This external voltage establishes an electric field perpendicular to the slot and causes index change in the infiltrated EO polymer. The unequal index induces different phase shift in two different arms of Mach-Zehnder modulator. When lights from both arms are recombined, interference between the two arms results in modulation of output signal. This change in output intensity was recorded with photo detector and shown in Figure 8. It shows sinusoidal like transfer curve with half-wave voltage (V_π) around 22V. The modulation depth of this modulator was found to be around 30%. The electro-optic coefficient can be calculated from the switching voltage with the following equation

$$\gamma_{33} = \frac{\lambda w}{n^3 V_\pi \Gamma L} \tag{1}$$

, where λ is the wavelength in free space, w is the distance between the center and side electrodes, n is the waveguide effective index, Vπ is the half-wave voltage, Γ is the overlap factor, and L is the electrode length. The overlapping factor Γ for the slot waveguide is taken to be ~0.3, the calculated electro-optic coefficient r33 is

$$\gamma_{33} = \frac{\lambda w}{n^3 V_\pi \Gamma L} = \frac{1495nm \times 332nm}{1.63^3 \times 22V \times 0.3 \times 340\mu m} = 51pm/V \tag{2}$$

This result is five times higher compared to recently reported in-device electro-optic coefficient [18].

6. CONCLUSION

In summary, we experimentally demonstrated a Mach-Zehnder modulator based on EO polymer infiltrated photonic crystal slot waveguide. The modulator shows a compact active length of only 352μm, which is benefited from the slow light enhancement of photonic crystal waveguide and the strong light confinement of slot waveguide. The device shows a switching voltage of 22V and in device EO coefficient of 51pm/V. The poling efficiency in nano-slot is still low compare to the results in thin film. With further optimization in poling process, it could lead to ultra compact device with extremely low power operation.

7. ACKNOWLEDGMENTS

This work is supported by AFOSR under contract number FA9550-09-C-0086 monitored by Dr. Charles Lee.

8. REFERENCE

[1] Y. Jiang, W. Jiang, L. Gu *et al.*, "80-micron interaction length silicon photonic crystal waveguide modulator," Applied Physics Letters, 87(22), 221105-3 (2005).
[2] G. Lanlan, J. Wei, C. Xiaonan *et al.*, "Thermooptically Tuned Photonic Crystal Waveguide Silicon-on-Insulator Mach-Zehnder Interferometers," Photonics Technology Letters, IEEE, 19(5), 342-344 (2007).
[3] T.-D. Kim, J. Luo, Y.-J. Cheng *et al.*, "Binary Chromophore Systems in Nonlinear Optical Dendrimers and Polymers for Large Electrooptic Activities," The Journal of Physical Chemistry C, 112(21), 8091-8098 (2008).
[4] M. Hochberg, T. Baehr-Jones, G. Wang *et al.*, "Terahertz all-optical modulation in a silicon-polymer hybrid system," Nat Mater, 5(9), 703-709 (2006).
[5] M. Notomi, K. Yamada, A. Shinya *et al.*, "Extremely Large Group-Velocity Dispersion of Line-Defect Waveguides in Photonic Crystal Slabs," Physical Review Letters, 87(25), 253902 (2001).
[6] S. John, "Strong localization of photons in certain disordered dielectric superlattices," Physical Review Letters, 58(23), 2486 (1987).
[7] E. Yablonovitch, "Inhibited Spontaneous Emission in Solid-State Physics and Electronics," Physical Review Letters, 58(20), 2059 (1987).
[8] A. Mekis, J. Chen, I. Kurland *et al.*, "High Transmission through Sharp Bends in Photonic Crystal Waveguides," Physical Review Letters, 77(18), 3787-3790 (1996).
[9] V. R. Almeida, Q. Xu, C. A. Barrios *et al.*, "Guiding and confining light in void nanostructure," Optics Letters, 29(11), 1209-1211 (2004).
[10] T. F. Krauss, "Slow light in photonic crystal waveguides," Journal of Physics D: Applied Physics, 40, 2666-2670 (2007).
[11] A. Di Falco, L. O'Faolain, and T. F. Krauss, "Photonic crystal slotted slab waveguides," Photonics and Nanostructures - Fundamentals and Applications, 6(1), 38-41 (2008).
[12] T. Baba, "Slow light in photonic crystals," Nature Photonics, 2(8), 465-473 (2008).
[13] N.-N. Feng, R. Sun, L. C. Kimerling *et al.*, "Lossless strip-to-slot waveguide transformer," Optics Letters, 32(10), 1250-1252 (2007).
[14] Z. Wang, N. Zhu, Y. Tang *et al.*, "Ultracompact low-loss coupler between strip and slot waveguides," Optics Letters, 34(10), 1498-1500 (2009).
[15] S. McNab, N. Moll, and Y. Vlasov, "Ultra-low loss photonic integrated circuit with membrane-type photonic crystal waveguides," Optics Express, 11(22), 2927-2939 (2003).
[16] Y. A. Vlasov, and S. J. McNab, "Coupling into the slow light mode in slab-type photonic crystal waveguides," Optics Letters, 31(1), 50-52 (2006).
[17] P. Pottier, M. Gnan, and R. M. De La Rue, "Efficient coupling into slow-light photonic crystal channel guides using photonic crystal tapers," Optic Express, 15(11), 6569-6575 (2007).
[18] J. H. Wulbern, J. Hampe, A. Petrov *et al.*, "Electro-optic modulation in slotted resonant photonic crystal heterostructures," Applied Physics Letters, 94(24), 241107-3 (2009).